

This discussion paper is/has been under review for the journal Atmospheric Chemistry and Physics (ACP). Please refer to the corresponding final paper in ACP if available.

CALIPSO observations of transatlantic dust: vertical stratification and effect of clouds

W. Yang¹, A. Marshak², T. Várnai³, O. V. Kalashnikova⁴, and A. B. Kostinski⁵

¹Goddard Earth Sciences Technology and Research, Universities Space Research Association, Columbia, MD 21044 USA

²NASA Goddard Space Flight Center, Greenbelt, MD 20771 USA

³Joint Center for Earth System Technology, University of Maryland at Baltimore County, Baltimore, MD 21228 USA

⁴Jet Propulsion Laboratory, 4800 Oak Grove Drive, Ms 180-401, Pasadena, CA 91109 USA

⁵Department of Physics, Michigan Technological University, Houghton, MI 49931 USA

Received: 16 March 2012 – Accepted: 24 April 2012 – Published: 10 May 2012

Correspondence to: W. Yang (weidong.yang@nasa.gov)

Published by Copernicus Publications on behalf of the European Geosciences Union.

Title Page

Abstract

Introduction

Conclusions

References

Tables

Figures

◀

▶

◀

▶

Back

Close

Full Screen / Esc

Printer-friendly Version

Interactive Discussion



Abstract

We use CALIOP nighttime measurements of lidar backscatter, color and depolarization ratios during the summer of 2007 to study transatlantic dust properties downwind of Saharan sources, and to examine the interaction of clouds and dust. Our analysis suggests that (1) while lidar backscatter doesn't change much with altitude in the Saharan Air Layer (SAL), depolarization and color ratios both increase with altitude in the SAL; (2) lidar backscatter and color ratio increase as dust is transported westward in the SAL; (3) the vertical lapse rate of dust depolarization ratio, introduced here, increases within SAL as plumes move westward; (4) nearby clouds barely affect the backscatter and color ratio of dust volumes within SAL but not so below SAL. Moreover, the presence of nearby clouds tends to decrease the depolarization of dust volumes within SAL. Finally, (5) the odds of CALIOP finding dust below SAL next to clouds are about 2/3 of those far away from clouds. This feature, together with an apparent increase in depolarization ratio near clouds, indicates that particles in some dusty volumes lose asphericity in the humid air near clouds, and cannot be identified by CALIPSO as dust.

1 Introduction

Atmospheric mineral dust particles have significant effects on the climate and the environment. Despite notable advances in modeling and satellite and ground-based measurements, dust remains the dominant factor in the uncertainty of aerosol radiative forcing (IPCC, 2001, 2007). Dust emitted from dry areas of Africa is transported over the North Atlantic Ocean to coastal areas of America with a peak of deposition during summer months (e.g., Prospero and Carlson, 1972; Mattsson and Nihlen, 1996; Prospero and Lamb, 2003; Torres et al., 2002; Kaufman et al., 2005).

The influence of dust on a radiative budget depends on its ability for absorbing and scattering solar and IR radiation. Dust optical properties are determined by the refractive index (i.e., chemical composition) (e.g., Sokolik and Toon, 1999; Wang et al., 2002;

[Title Page](#)

[Abstract](#)

[Introduction](#)

[Conclusions](#)

[References](#)

[Tables](#)

[Figures](#)

◀

▶

[Back](#)

[Close](#)

[Full Screen / Esc](#)

[Printer-friendly Version](#)

[Interactive Discussion](#)



Lafon et al., 2006; Kahnert et al., 2007; Kandler et al., 2007, 2009; Osborne et al., 2008; Petzold et al., 2009), size and shape of dust particles (Kalashnikova and Sokolik, 2002; Dubovik et al., 2006; Nousiainen, 2009). Dust hygroscopicity describes the particles' ability for taking up water from humid air, and is rooted in the physical-chemical properties of dust components. Dust is mostly composed of water-insoluble minerals and shows nearly complete hydrophobicity or at least poor hygroscopicity (e.g., Twomey, 1977; Li-Jones et al., 1998; Kaaden et al., 2009; Schladitz et al., 2011; Ansmann et al., 2011). However, after being lifted in the air and mixed/coated with water-soluble materials such as sea-salt, sulfate, or nitrate by atmospheric processing (Levin et al., 1996; 10 Yin et al., 2002), dust hygroscopicity can increase, which can cause changes in optical properties. In addition to mineral dust particles serving as ice nuclei (IN) (e.g., DeMott et al., 2003; Ansmann et al., 2008), the increase in hygroscopicity may also transform dust into effective cloud condensation nuclei (CCN) (Johnson, 1982; Wurzler et al., 2000; Sassen et al., 2003; Lohmann and Feichter, 2005; Twohy et al., 2009a) 15 and thereby affect the formation and distribution of clouds and precipitation (e. g. Kelly et al., 2007), thus also altering the radiative impact of clouds.

The evolving shape-dependent optical and hygroscopic properties of dust pose a question: how does the hygroscopicity of dust affect its optical properties near clouds? This question is pertinent as recent studies have shown that optical properties of clear sky aerosols are different in the vicinity of clouds from those far away from clouds (e.g., Clarke et al., 2002; Twohy et al., 2002, 2009b; Koren et al., 2007; Su et al., 2008; Redemann et al., 2009; Tackett and Girolamo, 2009; Várnai and Marshak, 2011). The answer to this question is likely not only to improve our understanding of dust-cloud interactions but also yield better estimates of direct radiative forcing. To that end, we present analysis of dust properties over the North Atlantic Ocean – including near-cloud behavior – based on Cloud-Aerosol Lidar with Orthogonal Polarization (CALIOP) data (Winker et al., 2003).

CALIOP is a space based lidar system onboard the Cloud Aerosol Lidar and Infrared Pathfinder Satellite Observations (CALIPSO) satellite launched in 2006. CALIOP data

Title Page	
Abstract	Introduction
Inclusions	References
Tables	Figures
◀	▶
◀	▶
Back	Close
Full Screen / Esc	
Printer-friendly Version	
Interactive Discussion	



offers many advantages for this study. First, since CALIOP uses a laser with a small footprint ($\sim 90\text{ m}$ in diameter on the ground), its aerosol data is not affected by the 3-D radiative enhancements of nearby clouds, which cause complications for instruments observing reflected sunlight (Wen et al., 2007; Marshak et al., 2008; Várnai and Marshak, 2011). Second, CALIOP provides backscatter depolarization information at 532 nm, which allows one to distinguish (typically) non-spherical dust from (typically) spherical droplets (Sassen, 2000; Murayama et al., 2001; Vaughan et al., 2004). Third, CALIOP's high spatial resolution (30 m vertically and 333 m horizontally) is well-suited for studying cloud-dust interactions that have typical scales of several kilometers (e.g., Koren et al., 2007; Várnai and Marshak, 2011).

2 Data and methodology

This study uses a month-long (7 June 2007–7 July 2007) dataset of nighttime CALIOP Version 3 data over the North Atlantic Ocean (0° N – 45° N , 0° W – 90° W). We note that since CALIPSO orbits are repeated in a 16-day cycle, our month-long dataset covers almost two orbital cycles, with the longitudes of closest orbits being 1.55° apart. Since in summer there are usually multiple outbreaks per month (Huang et al., 2010), this month-long dataset is sufficient to observe the basic features of dust outbreaks.

CALIOP measures the total backscatter of its laser pulses at 532 nm and 1064 nm wavelengths, and the perpendicularly polarized backscatter at 532 nm.

This paper characterizes dust particles using their attenuated backscatter coefficient (β'), attenuated color ratio (χ'), and depolarization ratio (δ') values. Unless specified otherwise, β' is the median of the vertically averaged 532 nm attenuated backscatter coefficients within dust layers identified by the 5 km-resolution aerosol product. χ' is the ratio between β' values at 1064 nm and 532 nm wavelengths, which tends to increase with the size of particles; this is especially true for optically small spherical particles. δ' is the ratio between the perpendicular and parallel components of β'_{532} , and is greater for non-spherical particles. We note that analyzing measured optical quantities helps

Title Page	
Abstract	Introduction
Conclusions	References
Tables	Figures
	
	
Back	Close
Full Screen / Esc	
Printer-friendly Version	
Interactive Discussion	



CALIPSO observations of transatlantic dust

W. Yang et al.

avoid potential artifacts that could be introduced by uncertainties in retrieving physical particle properties. However, we still use the results of operational CALIOP data processing for identifying cloud and dust layers. The operational algorithm identifies cloud and dust layers in three steps.

5 First, it identifies particle layers based on the observed 532 nm backscatter values (Winker et al., 2009; Vaughan et al., 2009).

Second, it determines whether a detected layer is a cloud or aerosol layer based on its latitude, altitude, 532 nm backscatter, color ratio and depolarization ratio (Liu et al., 2004, 2009). The most obvious clouds are identified at 333 m resolution, while the more ambiguous cases are decided at a coarser (1 km or 5 km) resolution. Our study considers a location cloudy if the 1 km resolution Level 2 CALIOP cloud product indicates the presence of clouds. In order to reduce the impact of misclassifications between clouds and aerosols, this paper examines aerosol layers only if the Cloud-Aerosol Discrimination (CAD) product (Liu et al., 2004, 2009) – based on probability distribution functions obtained from expert classifications for sample orbits – indicates that the likelihood of aerosol exceeds 70 %. As additional precaution, the statistical analysis in this paper examines median values instead of mean values, because medians are less sensitive to any outlying data points influenced by undetected cloud particles. The uncertainty of median values is estimated using the bootstrapping algorithm (Efron and Gong, 1983).

20 Third, the operational CALIOP data processing identifies dust layers as aerosol layers with high depolarization ratio values (Omar et al., 2009). Because depolarization depends on particle shape, it is well suited for separating typically non-spherical dust particles ($\delta' > 0.2$) from usually spherical non-dust aerosols ($\delta' < 0.075$) over ocean. We note that this paper considers dust-containing layers identified as either “dust” or
25 “polluted dust” in the 5 km-resolution level 2 aerosol product (polluted dust is dust mixed with biomass burning aerosols or polluted marine aerosols, with a depolarization ratio between those of dust and non-dust aerosols, 0.075 and 0.2, Omar et al., 2009).

To discern changes in dust properties during transatlantic transport, we examine dust behavior in the three regions shown in Fig. 1: East (E) (0° W– 30° W), Middle (M) (30° W–

Title Page	
ostract	Introduction
clusions	References
ables	Figures
◀	▶
◀	▶
Back	Close
Full Screen / Esc	
Printer-friendly Version	
Interactive Discussion	



60° W) and West (W) (60° W–90° W). These three regions lie at different distances from the African dust sources, and cover most of the dust paths from Africa to America during the summer of 2007.

3 Results and discussion

- 5 The spatial and optical characteristics of African dust vary during the transatlantic journey (e. g., Liu et al., 2008; Huang et al., 2010). In this section we examine the variations in three steps. First, the overall statistics of dust properties in the three geographic regions are compared. This part focuses on the vertical distribution of dust samples in the CALIOP 5 km resolution aerosol product, and on the vertical distributions of attenuated backscatter coefficient, color ratio and depolarization ratio. We then analyze the relationships between dust properties and cloud coverage in the three regions. Finally, we discuss the systematic changes in dust properties that occur near clouds.
- 10

3.1 Dust properties in the three regions

3.1.1 Vertical distribution of dust

- 15 Figure 2a shows the vertical distribution of dust samples in our three regions, normalized by the total number of dust samples within each region. The number of dust samples is defined as the number of 5 km long 270 m high volumes that, according to the CALIOP aerosol product, contain dust and have a CAD value between –70 and –100. In the eastern (E) region, more than 80 % of dust is between 1.5 km and 5.5 km
20 altitude, with the peak probability around 3.5 km. This elevated dust distribution is a typical result of two confining inversions below and above the SAL (Carlson and Prospero, 1972). The dust remains elevated in the middle (M) region as well, although the mean elevation descends about 0.5 km. The similar patterns in the E and M regions indicate that the updrafts keeping the dust at high altitudes in region E persist in region M as

[Title Page](#)

[Abstract](#)

[Introduction](#)

[Conclusions](#)

[References](#)

[Tables](#)

[Figures](#)

◀

▶

◀

▶

[Back](#)

[Close](#)

[Full Screen / Esc](#)

[Printer-friendly Version](#)

[Interactive Discussion](#)



well. If a 3-day average transport time from Region E to M is assumed, the descending velocity from center of E to center of M is estimated around 1.7 mms^{-1} , which is consistent with the typical SAL average descending velocity of $1\text{--}2 \text{ mm s}^{-1}$ (Carlson and Prospero, 1972). Finally, in the west (W) region the chances of finding dust decrease steadily with altitude, and dust is rarely found above 5 km. This dramatic change in the vertical distribution implies that the meteorological conditions in region W are different from those sustaining the elevated profiles in regions E and M. Moreover, the vertical distribution of dust in region W indicates that (dry and wet) dust sedimentation has the strongest impact over region W.

10 3.1.2 Attenuated backscatter coefficient, color ratio, and depolarization ratio of dust

This section examines dust optical properties in the three regions. Since dust above 5 km is rare, the analysis of dust optical properties will be limited to altitudes below 5 km. The analysis uses the Level 2 CALIOP aerosol layer product, which provides averaged β' , χ' , and δ' values for each dust layer. These layer-average values are assigned to all altitude bins within a dust layer when creating Fig. 2 (and 4).

The results in Fig. 2 show that dust properties vary with altitude differently within SAL (from 1.5 km to 5 km in altitude of regions E and M), below the SAL (below 1.5 km in regions E and M), and in region W.

In the SAL, median β'_{532} values are nearly constant with altitude, but the medians of χ' and δ' increase with altitude. Since the typically large and non-spherical dust particles imply large χ' and δ' values, the observed dusty volume behavior suggests that the concentration of dust increases with altitude and/or the concentration of non-dust marine aerosols in dusty volumes decreases with altitude.

Below the SAL in the E and M regions, the median δ' increases with altitude. This is the result of dust mixing with non-dust marine aerosols in the moist air confined between the marine surface and the inversion created by the dry and warm SAL aloft. Since the concentration of wet marine aerosols is much higher below than inside the

[Title Page](#)[Abstract](#)[Introduction](#)[Conclusions](#)[References](#)[Tables](#)[Figures](#)[◀](#)[▶](#)[◀](#)[▶](#)[Back](#)[Close](#)[Full Screen / Esc](#)[Printer-friendly Version](#)[Interactive Discussion](#)

SAL, backscatter from these aerosols contributes significantly to the lidar signals and reduce the depolarization ratios of dusty volumes below the SAL. As discussed in the following paragraph, the mixing of dust and marine aerosols in region W could be the major reason behind higher backscatter and lower depolarization in region W than in E or M.

In region W, the median of β'_{532} decreases with altitude and the medians of χ' and δ' increase with altitude up to at least 4–5 km. This behavior arises from the dissipation of the SAL in the region. As the SAL extends westward, its temperature drops and convection can bring in moist air from below. Eventually the inversion confining the moist marine air at low altitudes breaks up in region W, which allows the moist marine air to reach much higher altitudes. Even so, the concentration of wetter and larger marine aerosols tends to decrease with altitude, and so their contribution to the lidar backscatter of dusty volumes tends to be smaller at higher altitudes. This results in higher median χ' and δ' values at higher altitudes even in region W.

A comparison of dust properties in regions E, M, and W also reveals several features related to SAL influences at different transport stages. For example, at most altitudes the medians of β'_{532} and χ' increase westward, whereas the median of δ' tends to decrease westward. These trends arise from the fading of the SAL during the westward transport: as the air moves from west Africa to the Caribbean, the SAL temperature keeps decreasing, which allows the concentration of moist marine air mixed in from below to keep increasing. The presence of more moist marine aerosols at west increases the median β'_{532} and χ' of dusty volumes and reduces the median δ' value.

However, some features in Fig. 2 cannot be explained by contributions from non-dust marine aerosols in dusty sample volumes, and are likely caused by changes in the properties of dust particles instead. For example, Fig. 2d shows that above 3.5 km, the median δ' is larger in region M than in region E. This cannot be explained by mixing from below, because the larger contribution of mixed-in marine aerosols in region M would imply smaller (rather than larger) δ' values. Instead, the observed tendency is likely related to lower fall speed for aspherical dust particles: as the more spherical

CALIPSO observations of transatlantic dust

W. Yang et al.

[Title Page](#)

[Abstract](#)

[Introduction](#)

[Conclusions](#)

[References](#)

[Tables](#)

[Figures](#)

◀

▶

◀

▶

[Back](#)

[Close](#)

[Full Screen / Esc](#)

[Printer-friendly Version](#)

[Interactive Discussion](#)



particles fall faster, this leaves an increasingly non-spherical dust population at high altitudes as the air moves to region M. The plausibility of this scenario is also supported by simulations for highly irregular particles falling slower than more spherical ones, because of greater air resistance (Ginoux, 2003). This issue will be further discussed in Sect. 3.3.2.

We note that the slight increase of χ' of dusty volumes from E to M (in Fig. 2c) is different from the behavior of dust Angstrom exponents retrieved by MISR and MODIS, the latter displaying no significant changes during transatlantic transport (Kalashnikova and Kahn, 2008). This contrast is about vertical resolution: the CALIOP trend of westward increase in Fig. 2c occurs within SAL but MISR and MODIS integrate the entire atmospheric column and hence are affected by particles above and below SAL.

3.2 Correlation of dust properties with cloud fraction

This section examines the relationships between dust properties and cloudiness in the three study regions. We characterize cloudiness through the cloud fraction (CF), defined for each dust-containing 5 km-size column as the ratio of number of cloudy 0.333 km profiles to the total number of 0.333 km profiles in the column. Simply put, if the number of cloudy 0.333 km profiles is m , the cloud fraction is $m/15$. We note that in addition to the cloud fraction varying between 0 and 1, the relative location of dust and clouds within 5 km wide columns can also vary (Fig. 3). We also note that unlike the conventional cloud fraction that is based on 2-dimensional (2-D) images, our definition here is based on 1-dimensional (1-D) measurements along the CALIPSO track. Although off-track clouds may influence dust properties along the track even for $CF_{1D} = 0$ (Várnai and Marshak, 2012), CF_{1D} is still a generally useful indicator of cloud coverage.

The results in Fig. 4 show that dust properties are closely related to CF in all three regions. The main features of the relationship are as follows.

First, the top row of Fig. 4 reveals that a smaller fraction of dust samples occurs under clear skies in region M than in region E. This is because the SAL is warmer and

[Title Page](#)[Abstract](#)[Introduction](#)[Conclusions](#)[References](#)[Tables](#)[Figures](#)[◀](#)[▶](#)[◀](#)[▶](#)[Back](#)[Close](#)[Full Screen / Esc](#)[Printer-friendly Version](#)[Interactive Discussion](#)

**CALIPSO
observations of
transatlantic dust**

W. Yang et al.

[Title Page](#)[Abstract](#)[Introduction](#)[Conclusions](#)[References](#)[Tables](#)[Figures](#)[◀](#)[▶](#)[◀](#)[▶](#)[Back](#)[Close](#)[Full Screen / Esc](#)[Printer-friendly Version](#)[Interactive Discussion](#)

drier in the East, and so the conditions are less favorable for cloud formation in region E than region M.

Second, rows 2 and 3 in Fig. 4 reveal that within each region, the median values of β'_{532} and χ' are larger for higher CFs. This feature is likely caused by aerosols getting hydrated and swelling in humid regions containing clouds, although undetected cloud particles may also contribute. The figure also shows that in regions E and M, the increase in backscatter and color ratio is more pronounced below the SAL than inside it. The swelling is greater below the SAL than inside it both because clouds and high humidity are more common below the SAL, and because hygroscopic marine aerosols are fairly abundant at low altitudes even in dust layers, whereas the SAL is dominated by less hygroscopic dust particles.

Third, within each region, two opposite trends of correlations appear between δ' and CF: inside the SAL, the median δ' of dust is always larger in clear sky than in cloudy skies; whereas below the SAL, the median δ' of dust is always smaller in clear sky than in cloudy skies. The domains of these opposite behaviors can be separated in the fourth row of Fig. 4 roughly at the crossing point of the red curve (CF = 0) and the blue curve ($0 < \text{CF} < 0.6$). We note that these crossing points are approximately at the altitude of the bottom of the SAL. The opposite trends inside and below the SAL clearly indicate a different dust volume depolarization response to increased humidity. The possible mechanisms affecting the apparent depolarization ratio of dusty volumes below the SAL will be discussed in Sect. 3.4.

3.3 Features of dust volumes in the SAL under clear skies

Unlike the dusty volumes below the SAL, where the dust is mixed with humidified non-dust aerosols, the SAL is dominated by dust particles. This subsection examines several features of dust volumes inside the SAL in regions E and M. To reduce the effects of clouds, dust volumes are limited to only those under clear skies. In addition, region W is excluded because of its low number of dust samples inside the SAL (Fig. 2a).

3.3.1 Relationship of depolarization ratio with color ratio and backscatter

Figures 2 and 4 show that while backscatter is fairly uniform vertically, both color ratio and depolarization ratio increase markedly with altitude inside the SAL of regions E and M. These coinciding increases suggest systematic relationship between depolarization

- 5 ratio on the one hand and color ratio and backscatter on the other (Fig. 5). Figure 5a reveals a positive relationship between the depolarization ratio and color ratio of dust volumes in the SAL of regions E and M. In addition, the dynamic ranges of depolarization ratio and color ratio are much wider in region M than in region E. Figure 5b shows a similar relationship between depolarization ratio and backscatter, though with a much
10 smaller dynamic range for backscatter in region E. Figure 5c and d confirm that similar relationships are valid for a different dataset (covering 25 May 2008–25 June 2008) as well.

The relationships in Fig. 5 and the similarity of results from the two independent datasets can be attributed to the steady altitude-dependence of backscatter, color ratio and depolarization ratio inside the SAL. As discussed in Sect. 3.1.2, these altitude
15 dependences are likely caused by two mechanisms: (i) a decrease with altitude in the concentration of non-dust particles mixed in from below, and (ii) different fall speeds vertically separating the relatively more spherical dust particles from the least spherical ones. This latter mechanism dominates and is further explored in Sect. 3.3.2. In
20 addition, we note that the depolarization ratio is predominantly influenced by asphericity of the dust particles (e.g., Ansmann et al., 2003).

3.3.2 Relationship between the vertical increase in depolarization ratio and longitude

As indicated in Fig. 2, the depolarization ratio not only increases with altitude in the
25 SAL, but also has a larger increase rate in region M than E. As mentioned above, the increase may come from more spherical and less spherical dust particles getting vertically separated because of their different sedimentation speeds. The upward increase

[Title Page](#)[Abstract](#)[Introduction](#)[Conclusions](#)[References](#)[Tables](#)[Figures](#)[◀](#)[▶](#)[◀](#)[▶](#)[Back](#)[Close](#)[Full Screen / Esc](#)[Printer-friendly Version](#)[Interactive Discussion](#)

in δ' could then be stronger in region M simply because the sedimentation process has more time to work by the time the dust reaches region M.

Numerous studies have demonstrated that the fall speed of atmospheric particles depends on their shape (e.g., Chen et al., 1988; Ginoux, 2003) as well as size. Since particles with irregular shapes have greater cross-sectional areas and drag-coefficients, they experience stronger drag force in the air – which implies that more irregular particles of the same mass fall slower than more spherical ones. Note that a sphere is the most compact object (least surface area for a given volume) and it experiences least drag for a given mass. (Here we assume that dust particle shape does not change systematically with particle size, which also greatly impacts fall speed. This assumption is plausible because field experiments show distribution of aspect ratio is weakly related to particle size ,e.g., Chou et al., 2008; Kandler et al., 2009). As a result, shape-induced vertical separation will ensue as dust is advected westward, with irregular particles increasingly predominant in the upper portions of SAL. At a constant altitude, this stratification is expected to widen the dynamic range of depolarization ratios with downstream distance from the dust source. This is indeed the case.

To that end, we divide regions E and M into sub-regions covering 10° wide longitude bands, and examine the average difference between the depolarization ratios at 3 and 4 km altitudes for each region. As shown in Fig. 6, the average difference $\delta'_{4\text{ km}} - \delta'_{3\text{ km}}$ keeps increasing with the distance from the west coast of Africa. This result implies that the observed change in volume depolarization ratio within SAL is most likely caused by the greater drag of aspherical dust particles. In addition, this result is consistent with the observation of higher aspect ratio of long range transported Saharan dust (Reid et al., 2003a).

25 3.4 Dust volume properties near clouds

Relative humidity usually increases as clouds are approached and this causes nearby aerosols to swell and get hydrated (acquire thin film of water) or even activated as haze (e.g., Twohy et al., 2009b). Observing changes of dust characteristics near clouds can

[Title Page](#)[Abstract](#)[Introduction](#)[Conclusions](#)[References](#)[Tables](#)[Figures](#)[◀](#)[▶](#)[◀](#)[▶](#)[Back](#)[Close](#)[Full Screen / Esc](#)[Printer-friendly Version](#)[Interactive Discussion](#)

help improve our understanding of the effect of high relative humidity and clouds on dust particles. Figure 4 has shown that the backscatter and color ratio of dust volumes increase with cloud fraction both in and below the SAL, whereas the depolarization ratio changes with cloud fraction differently in and below the SAL. This finding indicates that 5 dust properties in and below the SAL are different. This section further examines the near cloud behaviors of dust volumes in and below the SAL. We note that although the base altitude of the SAL may vary during westward transport, as shown in Fig. 2 and 4, this analysis uses constant separation altitude of 2 km for convenience. The 10 analysis uses CALIOP Level 1 data to examine changes in backscatter, color ratio, and depolarization as a function of distance to clouds at a resolution of 0.333 km. In this analysis a 0.333 km resolution clear sky profile is considered a dusty profile if it is included in one or multiple 5 km resolution dust layer(s).

Figure 7 illustrates the behavior of dust as a function of distance to clouds. The orange curve corresponds to all aerosol samples while the black and green ones to high (in the SAL) and low (below the SAL) dust, respectively. Figure 7a shows that the 15 fraction of dust profiles over all detected aerosol profiles decreases dramatically near clouds for dust at altitudes below the SAL, but remains relatively stable for those in the SAL. The stable behavior in the SAL can be explained by the fact that low clouds confined to the boundary layer by the inversion at the base of the SAL have little impact on humidity inside the SAL. The near-cloud drop in the fraction of dust profiles below the SAL may result from several factors. First, the chances of wet removal are higher near clouds, and this can lower the fraction of dusty profiles. Second, swelling in the humid air near clouds makes particles more spherical (especially if water-soluble particles pollute dust crystals), resulting in the reduction of depolarization ratio thus 20 the dust signature (Omar et al., 2009); consequently, some dust-containing profiles are (mis)classified as non-dust aerosol. Assuming that below 2 km altitude, the fraction of dust profiles is constant beyond 5 km from clouds (as most humidity changes occur within 5 km from clouds), the roughly 2/3 drop in the fraction of dust profiles near clouds implies that at least 2/3 of dust profiles in the MBL are polluted and hygroscopic. This 25

**CALIPSO
observations of
transatlantic dust**

W. Yang et al.

[Title Page](#)[Abstract](#)[Introduction](#)[Conclusions](#)[References](#)[Tables](#)[Figures](#)[◀](#)[▶](#)[◀](#)[▶](#)[Back](#)[Close](#)[Full Screen / Esc](#)[Printer-friendly Version](#)[Interactive Discussion](#)

**CALIPSO
observations of
transatlantic dust**

W. Yang et al.

[Title Page](#)[Abstract](#)[Introduction](#)[Conclusions](#)[References](#)[Tables](#)[Figures](#)[|◀](#)[▶|](#)[◀](#)[▶|](#)[Back](#)[Close](#)[Full Screen / Esc](#)[Printer-friendly Version](#)[Interactive Discussion](#)

4 Summary

This paper uses CALIOP lidar data to examine the bulk optical properties of dust layers as Saharan dust moves westward over the Atlantic Ocean. It analyzes dust layers in three regions along the dust transport route, and examines the relationships between 5 dust properties and the amount and proximity of nearby clouds.

The study finds that the observed properties of dusty volumes are related not only to the meteorological conditions in the three regions, but also to the speed and duration of dry and wet sedimentation processes. The study examines four characteristics of 10 dust layers: (i) the volume of air containing dust, (ii) lidar backscatter (related to optical thickness), (iii) color ratio (roughly proportional to particle size) at least for spherical particles, and (iv) depolarization ratio (characterizing particle shape, with larger values for irregular particles than for spherical ones). The results show that lidar backscatter and color ratio are smaller, while the depolarization ratio is larger in the warmer and dryer east region.

15 The analysis reveals that the medians of depolarization ratio and color ratio generally increase with altitude in the SAL. The rate of vertical increase in depolarization ratio is significantly larger farther away from Africa's west coast.

We find the dusty volume optical properties related to cloud coverage, with backscatter and color ratio increase with cloudiness of surrounding areas. The effects of cloudiness are most prominent for dust below the SAL. The results highlight that sensitivity 20 to cloudiness is very different below and within SAL.

The results also reveal other differences between dust volume near-cloud behaviors inside and below the SAL. In the SAL, the fraction of aerosol samples that contain 25 dust doesn't depend on the distance to clouds, neither the median lidar backscatter, color ratio, and depolarization ratio. Below the SAL, the fraction of aerosol samples containing dust decreases near clouds, while the optical properties show noteworthy increases near clouds. The unique features of dust below the SAL indicate that in humid air near clouds only some large dust particles with much higher depolarization

[Title Page](#)[Abstract](#)[Introduction](#)[Conclusions](#)[References](#)[Tables](#)[Figures](#)[◀](#)[▶](#)[◀](#)[▶](#)[Back](#)[Close](#)[Full Screen / Esc](#)[Printer-friendly Version](#)[Interactive Discussion](#)

**CALIPSO
observations of
transatlantic dust**

W. Yang et al.

[Title Page](#)[Abstract](#)[Introduction](#)[Conclusions](#)[References](#)[Tables](#)[Figures](#)[◀](#)[▶](#)[Back](#)[Close](#)[Full Screen / Esc](#)[Printer-friendly Version](#)[Interactive Discussion](#)

ratio are identified as dust by the CALIPSO detection algorithm, and these particles become less frequent near clouds.

Earlier studies demonstrated that the degree of irregularity of dust affects dust optical properties and radiative forcing. Our observations further underline the need for assessing the effects of vertical separation in dust depolarization, caused by shape-dependent fall velocity, both in transport modeling and in estimating dust radiative forcing. In addition, our observations of near-cloud behaviors reveal the complexity of dust mixing with other water-soluble aerosols especially in the MBL, and support the hypothesis that dust, or the MBL part of it, becomes hygroscopic through interactions with atmospheric components in moist air, and this significantly affects dust optical properties.

Acknowledgements. We gratefully acknowledge support for this research by the NASA Radiation Sciences Program managed by Hal Maring, and by the NASA CALIPSO project supervised by Charles Trepte as the technical officer. This work was supported, in part, by NSF-AGS-1119164. We also wish to give special thanks to Drs. Peter R. Colarco, Ralph A. Kahn, Robert C. Levy, Zhaoyan Liu, Yuekui Yang, Hongbin Yu, Tianle Yuan, and other scientists at NASA GSFC for their helpful suggestions and fruitful discussions.

References

- Ansmann, A., Bösenberg, J., Chaikovsky, A., Comerón, A., Eckhardt, S., Eixmann, R., Freudenthaler, V., Ginoux, P., Komguem, L., Linné, H., Márquez, M. Á. L., Matthias, V., Mattis, I., Mitev, V., Müller, D., Music, S., Nickovic, S., Pelon, J., Sauvage, L., Sobolewsky, P., Srivastava, M. K., Stohl, A., Torres, O., Vaughan, G., Wandinger, U., and Wiegner, M.: Long-range transport of Saharan dust to Northern Europe: the 11–16 October 2001 outbreak observed with EARLINET, *J. Geophys. Res.*, 108, D244783, doi:10.1029/2003JD003757, 2003.
- Ansmann, A., Petzold, A., Kandler, K., Tegen, I., Wendisch, M., Müller, D., Weinzierl, B., Müller, T., and Heintzenberg, J.: Influence of Saharan dust on cloud glaciation in Southern Morocco during the Saharan mineral dust experiment, *J. Geophys. Res.*, 113, D04210, doi:10.1029/2007JD008785, 2008.

- Ansmann, A., Petzold, A., Kandler, K., Tegen, I., Wendisch, M., Müller, D., Weinzierl, B., Müller, T., and Heintzenberg, J.: Saharan mineral dust experiments SAMUM-1 and SAMUM-2: what have we learned?, *Tellus B*, 63, 403–429, 2011.
- Barber, R. T.: African dust and the demise of Caribbean Coral Reefs, *Geophys. Res. Lett.*, 27, 3029–3032, doi:10.1029/2000gl011599, 2000.
- Carlson, T. N. and Prospero, J. M.: The large-scale movement of Saharan air outbreaks over the Northern Equatorial Atlantic, *J. Appl. Meteorol.*, 11, 283–297, 1972.
- Cheng, Y.-S., Yeh, H.-C., and Allen, M. D.: Dynamic shape factor of a plate-like particle, *Aerosol Sci. Technol.*, 8, 109–123, 1988.
- Clarke, A. D., Howell, S., Quinn, P. K., Bates, T. S., Ogren, J. A., Andrews, E., Jefferson, A., and Massling, A.: INDOEX aerosol: a comparison and summary of chemical, microphysical, and optical properties observed from land, ship, and aircraft, *J. Geophys. Res.*, 107, D198033, doi:10.1029/2001JD000572, 2002.
- Chou, C., Formenti, P., Maille, M., Ausset, P., Helas, G., Harrison, M., and Osborne, S.: Size distribution, shape, and composition of mineral dust aerosols collected during the African Monsoon multidisciplinary analysis special observation period 0: dust and biomass-burning experiment field campaign in Niger, January 2006, *J. Geophys. Res.*, 113, D00C10, doi:10.1029/2008jd009897, 2008.
- DeMott, P. J., Sassen, K., Poellot, M. R., Baumgardner, D., Rogers, D. C., Brooks, S. D., Prenni, A. J., and Kreidenweis, S. M.: African dust aerosols as atmospheric ice nuclei, *Geophys. Res. Lett.*, 30, 1732, doi:10.1029/2003GL017410, 2003.
- Dubovik, O., Sinyuk, A., Lapyonok, T., Holben, B. N., Mishchenko, M., Yang, P., Eck, T. F., Volten, H., Muñoz, O., Veihelmann, B., van der Zande, W. J., Leon, J. F., Sorokin, M., and Slutsker, I.: Application of spheroid models to account for aerosol particle nonsphericity in remote sensing of desert dust, *J. Geophys. Res.*, 111, D11208, doi:10.1029/2005JD006619, 2006.
- Duce, R. A., Liss, P. S., Merrill, J. T., Atlas, E. L., Buat-Menard, P., Hicks, B. B., Miller, J. M., Prospero, J. M., Arimoto, R., Church, T. M., Ellis, W., Galloway, J. N., Hansen, L., Jickels, T. D., Knap, A. H., Reinhardt, K. H., Schneider, B., Soudine, A., Tokos, J. J., Tsunogai, S., Wollast, R., and Zhou, M.: The atmospheric input of trace species to the world ocean, *Global Biogeochem. Cy.*, 5, 193–259, 1991.
- Efron, B. and Gong, G.: A leisurely look at the bootstrap, the jackknife, and cross-validation, *Am. Statist.*, 37, 36–48, 1983.

[Title Page](#)[Abstract](#)[Introduction](#)[Conclusions](#)[References](#)[Tables](#)[Figures](#)[Back](#)[Close](#)[Full Screen / Esc](#)[Printer-friendly Version](#)[Interactive Discussion](#)

CALIPSO observations of transatlantic dust

W. Yang et al.

[Title Page](#)

[Abstract](#)

[Introduction](#)

[Conclusions](#)

[References](#)

[Tables](#)

[Figures](#)

◀

▶

[Back](#)

[Close](#)

[Full Screen / Esc](#)

[Printer-friendly Version](#)

[Interactive Discussion](#)



Ginoux, P.: Effects of nonsphericity on mineral dust modeling, *J. Geophys. Res.*, 108, D24052, doi:10.1029/2002JD002516, 2003.

Huang, J., Zhang, C., and Prospero, J. M.: African dust outbreaks: a satellite perspective of temporal and spatial variability over the tropical Atlantic Ocean, *J. Geophys. Res.*, 115, D05202, doi:10.1029/2009JD012516, 2010.

5 IPCC 2001: Climate Change 2001: The Scientific Basis, edited by: Houghton, J. T., Ding, Y., Griggs, D. J., Noguer, M., van der Linden, P. J., Dai, X., Maskell, K., and Johnson, C. A., Cambridge University Press, Cambridge, UK, 2001.

10 IPCC, 2007: Climate Change 2007: The Physical Science Basis, edited by: Solomon, S., Qin, D., Manning, M., Chen, Z., Marquis, M., Avery, K. B., Tignor, M., and Miller, H. L., Cambridge University Press, Cambridge, UK and New York, USA, 2007.

Johnson, D. B.: The role of giant and ultragiant aerosol particles in warm rain initiation, *J. Atmos. Sci.*, 39, 448–460, doi:10.1175/1520-0469(1982)039<0448:TROGAU>2.0.CO;2, 1982.

15 Kahnert, M., Nousiainen, T., and Raisanen, P.: Mie simulations as an error source in mineral aerosol radiative forcing calculations, *Q. J. Roy. Meteorol. Soc.*, 133, 299–307, 2007.

Kaaden, N., Massling, A., Schladitz, A., Müller, T., Kandler, K., Schütz, L., Weinzierl, B., Petzold, A., Tesche, M., Leinert, S., Deutscher, C., Ebert, M., Weinbruch, S., and Wiedensohler, A.: State of mixing, shape factor, number size distribution, and hygroscopic growth of the Saharan anthropogenic and mineral dust aerosol at Tinfou, Morocco, *Tellus B*, 61, 51–63, 2009.

20 Kalashnikova, O. V. and Kahn, R. A.: Mineral dust plume evolution over the Atlantic from MISR and MODIS aerosol retrievals, *J. Geophys. Res.*, 113, D24204, doi:10.1029/2008JD010083, 2008.

25 Kalashnikova, O. V. and Sokolik, I. N.: Importance of shapes and compositions of wind-blown dust particles for remote sensing at solar wavelengths, *Geophys. Res. Lett.*, 29, 1398, doi:10.1029/2007GL029253, 2002.

Kandler, K., Benker, N., Bundke, U., Cuevas, E., Ebert, M., Knippertz, P., Rodriguez, S., Schütz, L., and Weinbruch, S.: Chemical composition and complex refractive index of Saharan mineral dust at Izana, Tenerife (Spain) derived by electron microscopy, *Atmos. Environ.*, 41, 8058–8074, 2007.

30 Kandler, K., Schütz, L., Deutscher, C., Ebert, M., Hofmann, H., Jäckel, S., Jaenicke, R., Knippertz, P., Lieke, K., Massling, A., Petzold, A., Schladitz, A., Weinzierl, B., Wiedensohler, A., Zorn, S., and Weinbruch, S.: Size distribution, mass concentration, chemical and mineralog-

**CALIPSO
observations of
transatlantic dust**

W. Yang et al.

- ical composition and derived optical parameters of the boundary layer aerosol at Tinfou, Morocco, during SAMUM 2006, *Tellus B*, 61, 32–50, doi:10.1111/j.1600-0889.2008.00385.x, 2009.
- Kaufman, Y. J., Koren, I., Remer, L. A., Tanré, D., Ginoux, P. and Fan, S.: Dust transport and deposition observed from the Terra- Moderate Resolution Imaging Spectroradiometer (MODIS) spacecraft over the Atlantic Ocean, *J. Geophys. Res.*, 110, D10S12, doi:10.1029/2003JD004436, 2005.
- Kelly, J. T., Chuang, C. C., and Wexler, A. S.: Influence of dust composition on cloud droplet formation, *Atmos. Environ.*, 41, 2904–2916, 2007.
- Koren, I., Remer, L. A., Kaufman, Y. J., Rudich, Y., and Martins, J. V.: On the twilight zone between clouds and aerosols, *Geophys. Res. Lett.*, 34, L08805, doi:10.1029/2007JD009196, 2007.
- Lafon, S., Sokolik, I. N., Rajot, J. L., Caquineau, S., and Gaudichet, A.: Characterization of iron oxides in mineral dust aerosols: implications for light absorption, *J. Geophys. Res.*, 111, D21207, doi:10.1029/2005jd007016, 2006.
- Levin, Z., Ganor, E., and Gladstein, V.: The effects of desert particles with sulfate on rain formation in the Eastern Mediterranean, *J. Appl. Meteorol.*, 35, 1511–1523, 1996.
- Li-Jones, X., Maring, H. B., and Prospero, J. M.: Effect of relative humidity on light scattering by mineral dust aerosol as measured in the marine boundary layer over the tropical Atlantic Ocean, *J. Geophys. Res.*, 103, 31113–31121, 1998.
- Liu, Z., Vaughan, M., Winker, D., Hostetler, C. A., Poole, L. R., Hlavka, D. L., Hart, W. D., and McGill, M. J.: Use of probability distribution functions for discriminating between cloud and aerosol in lidar backscatter data, *J. Geophys. Res.*, 109, D15202, doi:10.1029/2004JD004732, 2004.
- Liu, Z., Omar, A., Vaughan, M., Hair, J., Kittaka, C., Hu, Y., Powell, K., Trepte, C., Winker, D., Hostetler, C., Ferrare, R., and Pierce, R.: CALIPSO lidar observations of the optical properties of Saharan dust: a case study of long-range transport, *J. Geophys. Res.*, 113, D07207, doi:10.1029/2007JD008878, 2008.
- Liu, Z., Vaughan, M. A., Winker, D. M., Kittaka, C., Kuehn, R. E., Getzewich, B. J., Trepte, C. R., and Hostetler, C. A.: The CALIPSO lidar cloud and aerosol discrimination: version 2 algorithm and initial assessment of performance, *J. Atmos. Oceanic Technol.*, 26, 1198–1213, doi:10.1175/2009JTECHA1229.1, 2009.

Title Page	
Abstract	Introduction
Conclusions	References
Tables	Figures
	
	
Back	Close
Full Screen / Esc	
Printer-friendly Version	
Interactive Discussion	



Lohmann, U. and Feichter, J.: Global indirect aerosol effects: a review, *Atmos. Chem. Phys.*, 5, 715–737, doi:10.5194/acp-5-715-2005, 2005.

Marshak, A., Wen, G., Coakley Jr., J. A., Remer, L. A., Loeb, N. G., Cahalan, R. F.: A simple model for the cloud adjacency effect and the apparent bluing of aerosols near clouds, *J. Geophys. Res.*, 113, D14S17, doi:10.1029/2007JD009196, 2008.

Mattsson, J. O. and Nihlen, T.: The transport of Saharan dust to Southern Europe: a scenario, *J. Arid Environ.*, 32, 111–119, doi:10.1006/jare.1996.0011, 1996.

Mishchenko, M. I. and Hovenier, J. W.: Depolarization of light backscattered by randomly oriented nonspherical particles, *Opt. Lett.*, 20, 1356–1358, 1995.

Murayama, T., Sugimoto, N., Uno, I., Kinoshita, K., Aoki, K., Hagiwara, N., Liu, Z., Matsui, I., Sakai, T., Shibata, T., Arao, K., Sohn, B. J., Won, J. G., Yoon, S. C., Li, T., Zhou, J., Hu, H., Abo, M., Iokibe, K., Koga, R., and Iwasaka, Y.: Ground-based network observation of Asian dust events of April 1998 in east Asia, *J. Geophys. Res.*, 106, 18346–18359, 2001.

Nousiainen, T.: Optical modeling of mineral dust particles: a review, *J. Quant. Spectrosc. Ra.*, 110, 1261–1279, 2009.

Omar, A. H., Winker, D., Kittaka, C., Vaughan, M., Liu, Z., Hu, Y., Trepte, C., Rogers, R., Ferrell, R., Lee, K.-P., Kuehn, R., and Hostetler, C.: The CALIPSO automated aerosol classification and lidar ratio selection algorithm, *J. Atmos. Oceanic Technol.*, 26, 1994–2014, doi:10.1175/2009JTECHA1231.1, 2009.

Osborne, S. R., Johnson, B. T., Haywood, J. M., Baran, A. J., Harrison, M. A. J., and McConnell, C. L.: Physical and optical properties of mineral dust aerosol during the dust and biomass-burning experiment, *J. Geophys. Res.*, 113, D00C03, doi:10.1029/2007JD009551, 2008.

Petzold, A., Rasp, K., Weinzierl, B., Esselborn, M., Hamburger, T., Dörnbrack, A., Kandler, K., Schütz, L., Knippertz, P., Fiebig, M., and Virkkula, A.: Saharan dust absorption and refractive index from aircraft-based observations during SAMUM 2006, *Tellus B*, 61, 118–130, doi:10.1111/j.1600-0889.2008.00383.x, 2009.

Prospero, J. M. and Carlson, T. N.: Vertical and areal distribution of Saharan dust over the Western Equatorial North Atlantic Ocean, *J. Geophys. Res.*, 77, 5255–5265, 1972.

Prospero, J. M. and Lamb, P. J.: African droughts and dust transport to the Caribbean: climate change implications, *Science*, 302, 1024–1027, 2003.

CALIPSO
observations of
transatlantic dust

W. Yang et al.

[Title Page](#)

[Abstract](#)

[Introduction](#)

[Conclusions](#)

[References](#)

[Tables](#)

[Figures](#)

◀

▶

◀

▶

[Back](#)

[Close](#)

[Full Screen / Esc](#)

[Printer-friendly Version](#)

[Interactive Discussion](#)



CALIPSO observations of transatlantic dust

W. Yang et al.

- Redemann, J., Zhang, Q., Russell, P. B., Livingston, J. M., and Remer, L. A.: Case studies of aerosol remote sensing in the vicinity of clouds, *J. Geophys. Res.*, 114, D06209, doi:10.1029/2008JD010774, 2009.
- Sassen, K.: The lidar backscatter depolarization technique for cloud and aerosol research, in: Light Scattering by Nonspherical Particles: Theory, Measurements, and Geophysical Applications, edited by: Mishchenko, M. L., Hovenier, J. W., and Travis, L. D., Academic, San Diego, California, 2000.
- Sassen, K., DeMott, P. J., Prospero, J. M., and Poellot, M. R.: Saharan dust storms and indirect aerosol effects on clouds: CRYSTAL-FACE results, *Geophys. Res. Lett.*, 30, 1633–1636, doi:10.1029/2003GL017371, 2003.
- Schloditz, A., Müller, T., Nowak, A., Kandler, K., Lieke, K., Massling, A., and Wiedensohler, A.: In-situ aerosol characterization at Cape Verde, part 1: particle number size distributions, hygroscopic growth, and state of mixing of the marine and Saharan dust aerosol, *Tellus B*, 63, 531–548, 2011.
- Sokolik, I. and Toon, O.: Incorporation of mineralogical composition into models of the radiative properties of mineral aerosol from UV to IR wavelengths, *J. Geophys. Res.*, 104, 9423–9444, 1999.
- Su, W., Schuster, G. L., Loeb, N. G., Rogers, R. R., Ferrare, R. A., Hostetler, C. A., Hair, J. W., and Obland, M. D.: Aerosol and cloud interaction observed from high spectral resolution lidar data, *J. Geophys. Res.*, 113, D24202, doi:10.1029/2009GL039264, 2008.
- Torres, O., Bhartia, P. K., Herman, J. R., Sinyuk, A., Ginoux, P., and Holben, B.: A long-term record of aerosol optical depth from TOMS observations and comparison to AERONET measurements, *J. Atmos. Sci.*, 59, 398–413, 2002.
- Tackett, J. L. and Girolamo, L. D.: Enhanced aerosol backscatter adjacent to tropical trade wind clouds revealed by satellite-based lidar, *Geophys. Res. Lett.*, 36, L14804, doi:10.1029/2001JD001544, 2009.
- Twohy, C. H., Clement, C. F., Gandrud, B. W., Weinheimer, A. J., Campos, T. L., Baumgardner, D., Brune, W. H., Faloona, I., Sachse, G. W., Vay, S. A., and Tan, D.: Deep convection as a source of new particles in the midlatitude upper troposphere, *J. Geophys. Res.*, 107, D214560, doi:10.1029/2001JD000323, 2002.
- Twohy, C. H., Kreidenweis, S. M., Eidhammer, T., Browell, E. V., Heymsfield, A. J., Bansemer, A. R., Anderson, B. A., Chen, G., Ismail, S., DeMott, P. J., and Van Den Heever, S. C.:

Title Page	
Abstract	Introduction
Conclusions	References
Tables	Figures
	
	
Back	Close
Full Screen / Esc	
Printer-friendly Version	
Interactive Discussion	



**CALIPSO
observations of
transatlantic dust**

W. Yang et al.

- Saharan dust particles nucleate droplets in Eastern Atlantic clouds, *Geophys. Res. Lett.*, 36, L01807, doi:10.1029/2008GL035846, 2009a.
- Twohy, C. H., Coakley Jr., J. A., and Tahnk, W. R.: Effect of changes in relative humidity on aerosol scattering near clouds, *J. Geophys. Res.*, 114, D05205, doi:10.1029/2008JD010991, 2009b.
- Towmey, S.: *Atmospheric Aerosols*, Elsevier North-Holland Inc., New York, 1977.
- Várnai, T. and Marshak, A.: Global CALIPSO observations of aerosol changes near clouds, *IEEE Rem. Sens. Lett.*, 8, 19–23, 2011.
- Várnai, T. and Marshak, A.: Analysis of co-located MODIS and CALIPSO observations near clouds, *Atmos. Meas. Tech.*, 5, 389–396, doi:10.5194/amt-5-389-2012, 2012.
- Vaughan, M. A., Young, S., Winker, D., Powell, K., Omar, A., Liu, Z., Hu, Y., and Hostetler, C.: Fully automated analysis of space-based lidar data: an overview of the CALIPSO retrieval algorithms and data products, in: *Laser Radar Techniques for Atmospheric Sensing*, edited by Singh, U. N., *Proceedings of SPIE*, SPIE, 5575, 16–30, doi:10.1117/12.572024, Bellingham, WA, 2004.
- Vaughan, M. A., Powell, K., Kuehn, R., Young, S., Winker, D., Hostetler, C., Hunt, W., Liu, Z., McGill, M., and Getzewich, B.: Fully automated detection of cloud and aerosol layers in the CALIPSO lidar measurements, *J. Atmos. Oceanic Technol.*, 26, 2034–2050, doi:10.1175/2009JTECHA1228.1, 2009.
- Wang, J., Flagan, R. C., Seinfeld, J. H., Jonsson, H. H., Collins, D. R., Russell, P. B., Schmid, B., Redemann, J., Livingston, J. M., Gao, S., Hegg, D. A., Welton, E. J., and Bates, D.: Clear-column radiative closure during ACE-Asia: comparison of multiwavelength extinction derived from particle size and composition with results from sun photometry, *J. Geophys. Res.*, 107, 4688, doi:10.1029/2002JD002465, 2002.
- Wen, G., Marshak, A., Cahalan, R. F., Remer, L. A., and Kleidman, R. G.: 3-D aerosol-cloud radiative interaction observed in collocated MODIS and ASTER images of cumulus cloud fields, *J. Geophys. Res.*, 112, D13204, doi:10.1029/2006JD008267, 2007.
- Winker, D. M., Pelon, J. R., and McCormick, M. P.: The CALIPSO mission: spaceborne lidar for observation of aerosols and clouds, in: *Proc. SPIE* 4893, 1, doi:10.1117/12.466539, 1–11, 2003.
- Winker, D. M., Vaughan, M. A., Omar, A., Hu, Y., Powell, K. A., Liu, Z., Hunt, W. H., Young, S. A.: Overview of the CALIPSO mission and CALIOP data processing algorithms, *J. Atmos. Oceanic Technol.*, 26, 2310–2323, doi:10.1175/2009JTECHA1281.1, 2009.

Title Page	
Abstract	Introduction
Conclusions	References
Tables	Figures
	
	
Back	Close
Full Screen / Esc	
Printer-friendly Version	
Interactive Discussion	



**CALIPSO
observations of
transatlantic dust**

W. Yang et al.

[Title Page](#)[Abstract](#)[Introduction](#)[Conclusions](#)[References](#)[Tables](#)[Figures](#)[◀](#)[▶](#)[◀](#)[▶](#)[Back](#)[Close](#)[Full Screen / Esc](#)[Printer-friendly Version](#)[Interactive Discussion](#)

**CALIPSO
observations of
transatlantic dust**

W. Yang et al.

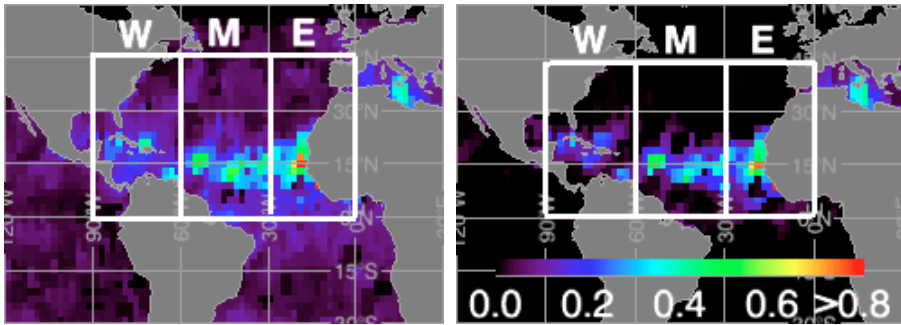


Fig. 1. Location of the 3 North-Atlantic regions examined in this study. Colors indicate the night-time CALIOP Aerosol Optical Depth (AOD) contributed from all aerosols (left), and contributed from dust aerosols (right) over oceans for the 7 June–7 July, 2007 period, at a pixel resolution of $2^\circ \times 2^\circ$.

[Title Page](#)[Abstract](#)[Introduction](#)[Conclusions](#)[References](#)[Tables](#)[Figures](#)[|◀](#)[▶|](#)[◀](#)[▶|](#)[Back](#)[Close](#)[Full Screen / Esc](#)[Printer-friendly Version](#)[Interactive Discussion](#)

CALIPSO observations of transatlantic dust

W. Yang et al.

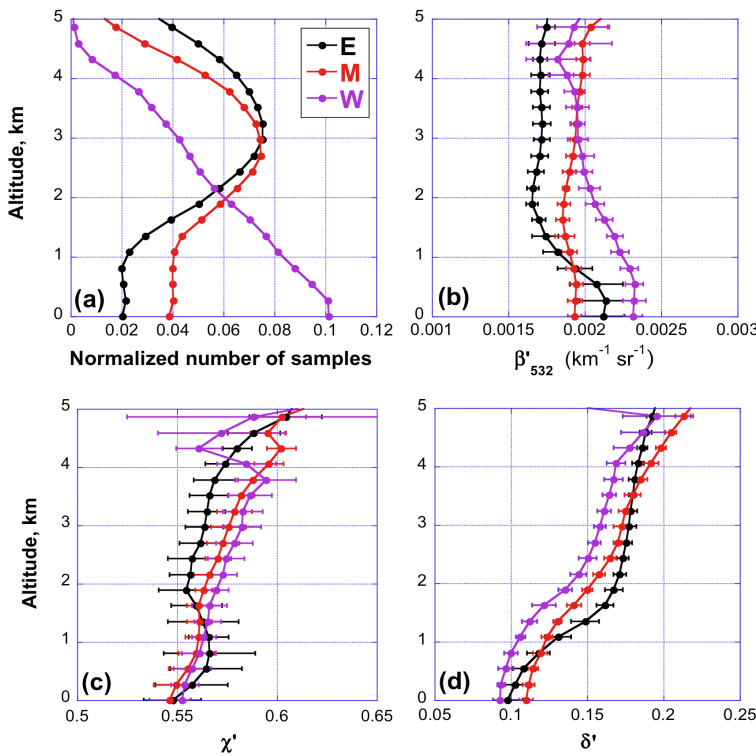


Fig. 2. Vertical profiles of (a) number of 5 km-resolution dust samples, normalized by the total number of dust samples at each corresponding region. The total number of dust samples is 45 714 for E, 73 141 for M and 32 785 for W. In addition, the E, M, and W regions contain 24 701, 34 019, and 23 786 5 km-resolution vertical profiles over ocean, respectively. (b) median attenuated total backscatter coefficient at 532 nm, β'_{532} , (c) median attenuated color ratio, χ' , (d) median volume depolarization ratio, δ' . The colors identify the profiles for each study region (east, middle, and west). The error bars indicate the uncertainty of median values, estimated using the bootstrap algorithm.

- [Title Page](#)
- [Abstract](#) [Introduction](#)
- [Conclusions](#) [References](#)
- [Tables](#) [Figures](#)
- [◀](#) [▶](#)
- [◀](#) [▶](#)
- [Back](#) [Close](#)
- [Full Screen / Esc](#)
- [Printer-friendly Version](#)
- [Interactive Discussion](#)

**CALIPSO
observations of
transatlantic dust**

W. Yang et al.

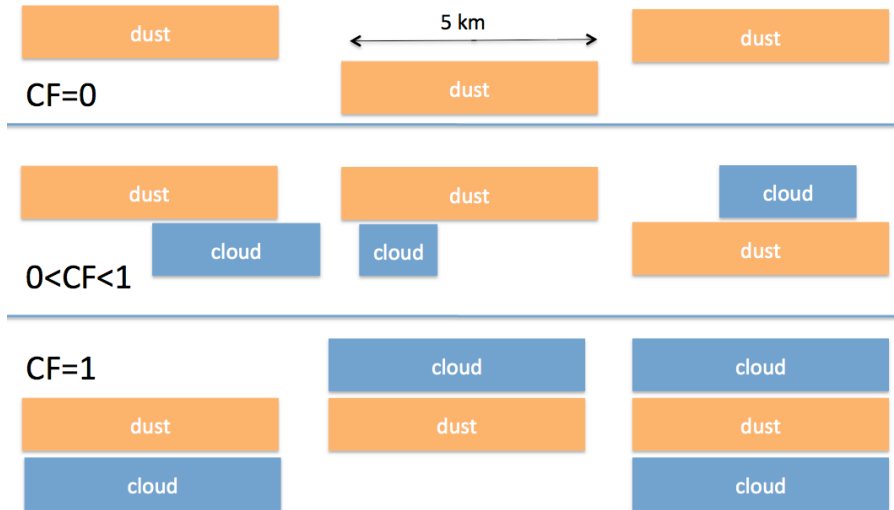


Fig. 3. Schematic illustration of cloud fraction (CF) definitions for 5 km resolution dust pixels. CF is the fraction of cloudy 0.3 km-resolution pixels in 5 km size areas containing dust.

CALIPSO observations of transatlantic dust

W. Yang et al.

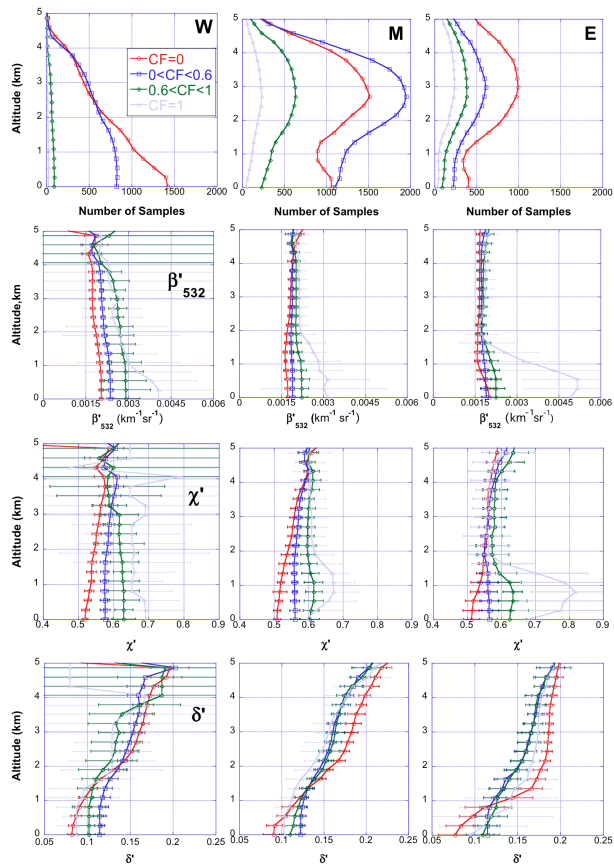


Fig. 4. Vertical profiles of dust properties for various cloud fractions at the 3 regions. Rows 1, 2, 3 and 4 are for frequency of occurrence, attenuated total backscatter coefficient at 532 nm, β'_{532} , attenuated color ratio, χ' , and volume depolarization ratio, δ' , respectively. The left, center, and right columns show the west, middle and east regions, respectively. Results for different cloud fractions are indicated by different colors.

[Title Page](#)

[Abstract](#)

[Introduction](#)

[Conclusions](#)

[References](#)

[Tables](#)

[Figures](#)



[Back](#)

[Close](#)

[Full Screen / Esc](#)

[Printer-friendly Version](#)

[Interactive Discussion](#)

CALIPSO observations of transatlantic dust

W. Yang et al.

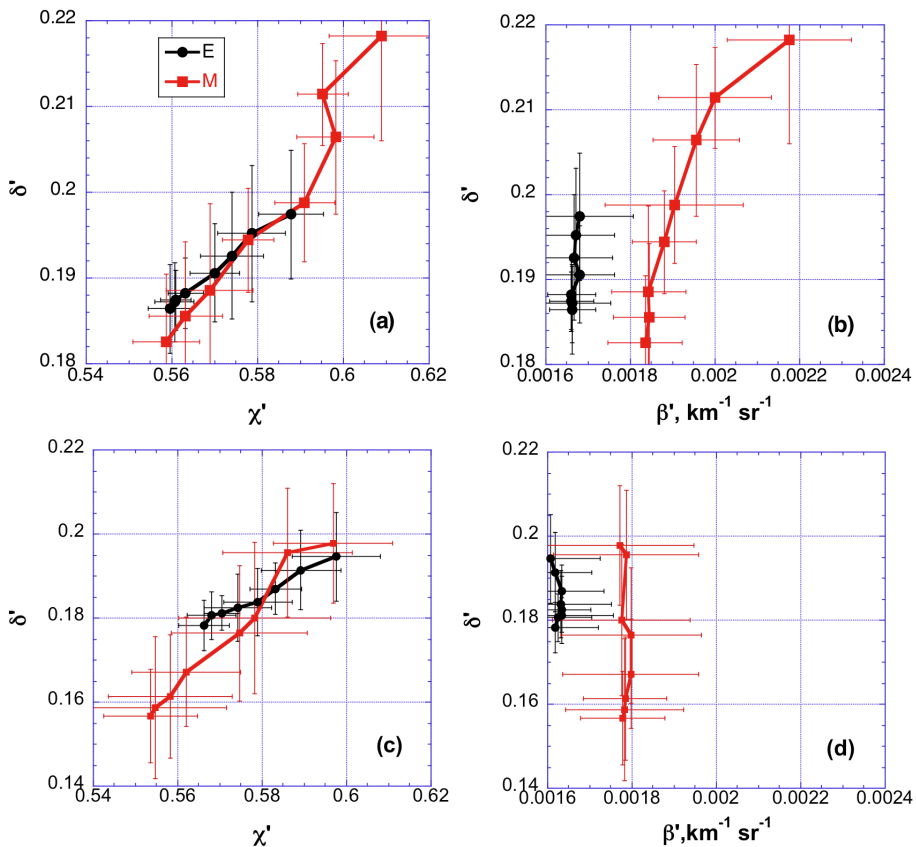


Fig. 5. Median depolarization ratio, δ' , as a function of color ratio, χ' **(a)**, and backscatter coefficient, β'_{532} **(b)**. As in Fig. 2, colors identify the examined regions E (black) and M (red). **(c)** and **(d)** are the same as **(a)** and **(b)**, but for a different dataset from 25 May to 25 June of 2008.

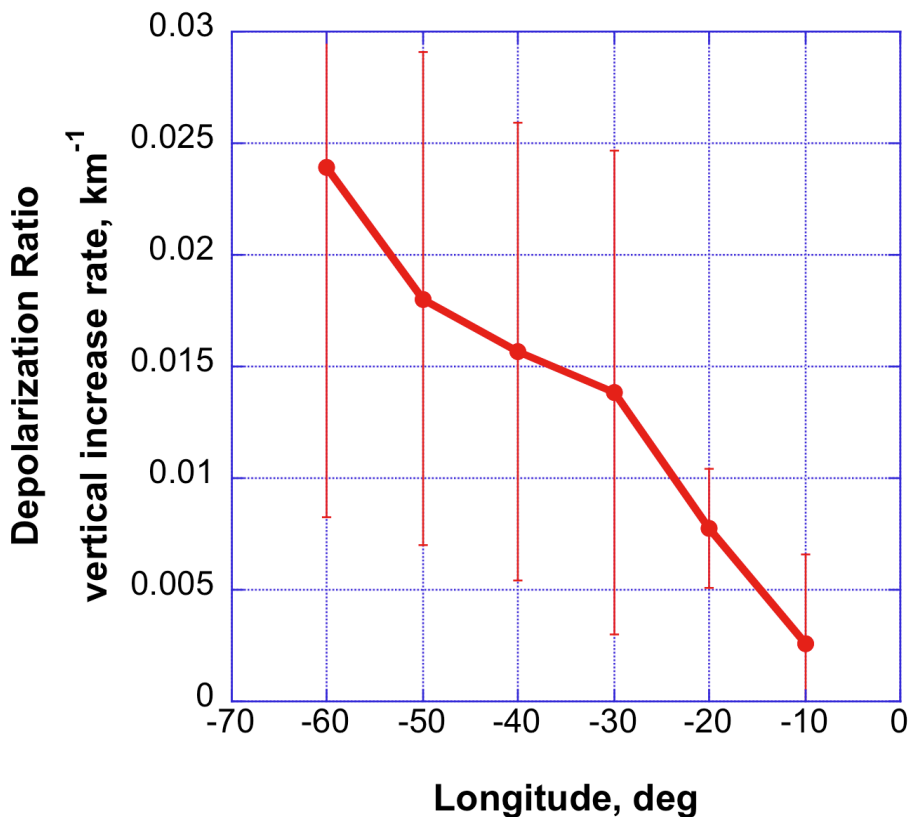


Fig. 6. Rate of vertical increase in dust depolarization ratio between 3 km and 4 km altitudes, vs. distance from the African coast, represented by longitude. Particle shape-dependent differences in fall speed cause increasingly more pronounced vertical stratification as plumes move westward.

CALIPSO observations of transatlantic dust

W. Yang et al.

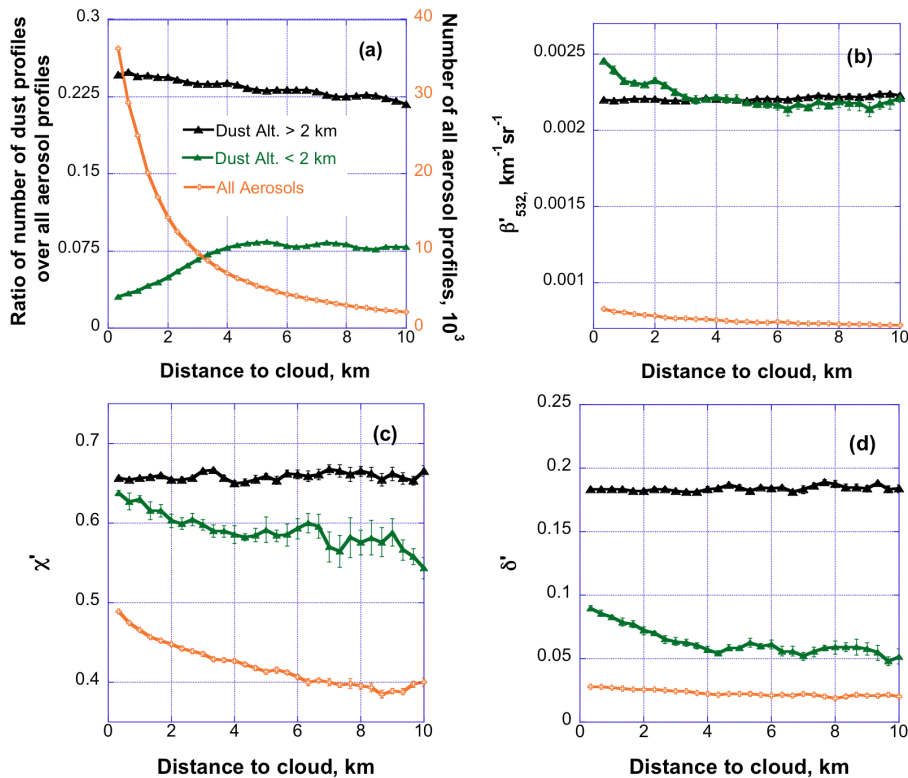


Fig. 7. Properties of high and low dust as a function of distance to clouds, combined for the three regions (W + M + E): **(a)** fraction of detected aerosol profiles that contain dust, **(b)** attenuated backscatter coefficient at 532 nm, β'_{532} , **(c)** attenuated color ratio, χ' , **(d)** depolarization ratio, δ' . The orange curve in **(a)** is the number of detected “all aerosol” profiles as a function of distance to clouds. It is also used as denominator in calculating the fraction of high and low dust profiles. Orange curves in **(b)–(d)** show the optical properties of all aerosols combined.

Title Page	Abstract	Introduction
Conclusions	References	
Tables	Figures	
◀	▶	
◀	▶	
Back	Close	
Full Screen / Esc		
Printer-friendly Version		
Interactive Discussion		

